

Fracture Property evaluation of X100 Pipeline Steel: Combined Experimental-Numerical Process^a

M. Szanto^b, C.N. McCowan^c, E.S. Drexler^c, and J.D. McColskey^c

Abstract

Accurate characterization of material fracture properties is necessary for reliable numerical prediction of rupture in gas pipelines. In the current work, the ductile fracture properties for high strength X100 pipeline steel were evaluated with experimental data from a single type of experiment. The material characterization was based on a combination of experimental results with numerical simulation for a modified double cantilever beam (MDCB) specimen. The material properties were obtained by parametrical adjustments of the numerical results to the experimental measurements at points along the propagation of a crack in the specimen. The values of the equivalent plastic strain and the stress triaxiality (ratio of the pressure stress to the equivalent stress) were computed at the crack tip for different crack lengths. The fracture properties were evaluated parametrically through an adjustment between the experimental and the computational force-displacement curves. Damage at fracture initiation was considered as a function of the stress triaxiality and plastic strain rate at quasi static and dynamic testing rates. The numerical computations were performed with a commercial finite element code.

Introduction

Fracture in high strength steels is classified into two main categories, brittle and ductile. Brittle fracture is characterized by breaking of inter-atomic bonds without plastic deformation. Ductile fracture is characterized by void nucleation, growth, and coalescence and is a cumulative process. Employing continuum mechanics for the fracture analysis, the microscopic failure is translated into a macroscopic parametrical model accumulating an equivalent failure strain. In the current work, failure is characterized by a damage initiation function with the state of stress, strain rate, temperature, and other parameters such as anisotropy [1-5]. After damage initiation in an element, the evolution is characterized by progressive degradation of the material stiffness up to complete failure of the material. A complete failure is equivalent to removal of an element from the computation.

For the ductile damage initiation, several phenomenological models are available. All of the models make use of more than one parameter. In the current work, the Johnson-Cook model [1] was the primary model considered. In order to characterize the parameters of the model, loads were applied that induced simple stress states. Nevertheless, the stress state in the vicinity of damage is complex and more difficult to predict.

^a Contribution of NIST, an agency of the US government; not subject to copyright in the United States.

^b Nuclear Research Centre-Negev, P.O.B. 9001, Beer-Sheva, Israel

^c NIST, Materials Reliability Division, 325 Broadway, Boulder Colorado

The objective of the present work is to evaluate the ductile fracture properties of high strength X100 pipeline steel, as a basis toward a reliable characterization of damage in pipelines. The material fracture characterization was based on a single type of experiment, with a modified-double-cantilever-beam (MDCB) specimen [5-9]. A full parametrical identification was carried out with results from several different points during the extension of the crack. The parameter identification was done in a combined experimental-numerical approach by minimizing the difference between the predicted force-displacement curve along the crack length with use of the experimentally measured curve. The numerical computations were performed with a commercial finite element method (FEM) code.

Experimental setup

CTOA (Crack Tip Opening Angle) tests were conducted with MDCB specimens [5-9, 10]. The test specimens were extracted from the pipe so that the crack growth direction was along the length of the pipe. The MDCB configuration and dimensions are depicted in **Figure 1**.

The large in-plane dimensions of the specimens (200 mm × 100 mm) and the long ligament allows relatively large amounts of stable crack growth. As shown in **Figure 1**, the specimen has a reduced thickness test section (8 mm) with a machined notch and mounting holes for a clip gauge. The machined notch length and width were 60 mm and 1.6 mm, respectively. At the end of the machine notch, an 8 mm EDM wire cut was added. The EDM wire diameter was 0.3 mm.

The loading configuration for the specimens is shown in **Figure 2**. The two cylindrical loading pins provide free rotation of the whole assembly during the experiment. The reduced middle section together with the two loading plates increased the constraint levels in the gauge section. The long, uncracked ligament and the loading geometry provided a condition of stable crack extension in the specimen ligament, similar to that of the real pipeline structure. The load-line passes through the left pair of loading holes. The plate grips generate frictional force that holds together the loading plates and the specimen.

The tests were displacement controlled, with force measured by a load cell. The specimen displacement was measured by two methods: (1) a linear variable differential transformer (LVDT) on the actuator of the load frame and (2) a crack mouth opening displacement (CMOD) clip gauge near the machined notch on the specimen.

Both quasi static and dynamic experiments were performed. The quasi static experiments were conducted on a 250 kN closed-loop servo-hydraulic test machine under opening (mode I) loading, with the displacement control rate in the range of 0.002 mm/s to 0.02 mm/s. The dynamic experiments were conducted on a 500 kN machine at a displacement velocities of 300 mm/s. In each test, time, force, and load

line displacement were recorded by CMOD gauge. Data for five quasi static tests and one dynamic test are reported. The specimens were either pre-cracked following the ASTM standard procedure for conducting crack tip opening displacement (CTOD) tests [ASTM E 1820, $R = 0.1$, $a_0/W = 0.3$ to 0.5], or specimens were cut with electrical discharge machining (EDM) to simulate fatigue crack extension.^a

Computational model

The overall goal is to construct a numerical tool for modeling crack initiation and dynamic crack propagation in pipeline steels. In the model presented here, two types of possible damage initiation assumptions are built in. The first is a result of ductile fracture (due to nucleation and growth), while the second is a result of shear fracture (due to shear band localization).

A combination of damage initiation assumptions is possible. However, evaluations of cross sections ground through to the crack plane (**Figure 3**) show a simple case. Voids not yet fully connected to the crack are present in front of the crack tip and as the crack advances the isolated voids are connected and the crack tip is extended. This is a typical ductile fracture mechanism consisting of nucleation and void growth. There is no experimental evidence of shear fracture in the macro-sense, where void sheet coalescence results in the formation of shear-lips at the outside surface of the specimens. Therefore, in the current model, only a ductile damage initiation mechanism was considered.

In **Figure 4**, the characteristic fracture morphologies for the CTOA specimens are shown in cross section. Ideally, the specimens fail with either a slant or flat macroscopic failure orientation, but combinations of these morphologies are common in both laboratory specimens and full-scale pipeline failures. The slant-type fractures in **Figure 4a and b** show that slant fractures occur on single and double planes [10]. The classic flat fracture in **Figure 4c** shows that the central region of the specimen thickness is basically on a plane perpendicular to the loading direction. There is very little shear fracture associated with either of these fracture morphologies. In the slant fractures, shear regions typically only extend in from the outside surface of the specimens to a depth of less than 10 % of the specimen thickness (sometimes more like 1 %). For flat fractures, the morphology is cup-cup in cross section rather than cup-cone. The final fracture region near the outside surface of the specimens is not formed by a shear band localization mechanism. The material flows in a general plastic manner that results in a knife-edge like fracture rather than a shear lip.

^a Our data has shown no differences in force-displacement curves between specimens tested with fatigue and EDM crack extensions, and no differences in the plastic deformation have been apparent on the gridded surfaces of the specimens during crack initiation or growth. However, differences in the details of fracture initiation were not evaluated in detail and should not be dismissed. Following several millimeters of crack growth, no differences in fracture are anticipated.

After ductile damage initiation, the model evolution is characterized by degradation of the material (reduction of the stiffness) up to complete material failure, *i.e.* the element stiffness reduces to zero, and crack extension is completed through the whole element. At complete failure, the element is removed from the computation, and the crack tip is advanced a distance equal to the length of the element removed. This approach is justified when the elements are small at the vicinity of the crack, and the element removal can be considered similar to material removal due to the nucleation, growth and coalescence of voids.

There are alternative applicable approaches for numerical prediction of crack propagation based on measures of the energy release rate by the crack propagation, computed at or around the crack tip combined with finite element approaches [14,15]. One of the prevalent approaches in the gas transmission industry is based on the CTOA [11-13]. Crack extension occurs when the CTOA exceeds its experimentally determined critical value.

The key point in an accurate prediction of damage is an adequate model for crack initiation. The simplest model defines fracture at a point when the equivalent plastic strain $\varepsilon_{eq_D}^{pl}$, reaches its critical value ε_{crit} .

For an incompressible material in the plastic regime:

$$1) \quad \varepsilon_{eq_D}^{pl} = \sqrt{\frac{2}{3}(\varepsilon_i \varepsilon_i)}$$

Where: ε_i , $i=1-3$, are the principal strains.

While this criterion is simple to adopt in computational codes, it lacks generality. The main drawback is that differences between compressive and tensile strains are not distinguished. Since void growth and coalescence is always expected to increase under critical tension loads and could decrease under similar magnitude compression loading, fracture could occur at considerably different levels of tensile and compressive strain. Hence, ductile fracture is pressure dependent.

The dependency of the ductile fracture on pressure is considered, in various models, by the stress triaxiality η , defined as the ratio of the pressure stress to the equivalent stress (usually Von-Mises stress) [1]:

$$2) \quad \eta = \frac{\sigma_m}{\sigma_{VM}} = \frac{\sigma_1 + \sigma_2 + \sigma_3}{3 \sqrt{\frac{1}{2}(\sigma_1 - \sigma_2)^2 + \sigma_2 - \sigma_3)^2 + \sigma_3 - \sigma_1)^2}}$$

or as [2]:

$$3) \quad \eta = \frac{3\sigma_m}{\sigma_{VM}} = \frac{\sigma_1 + \sigma_2 + \sigma_3}{\sqrt{\frac{1}{2}(\sigma_1 - \sigma_2)^2 + \sigma_2 - \sigma_3)^2 + \sigma_3 - \sigma_1)^2}}$$

where σ_i ($i=1-3$) are the principal stresses.

As the result of nucleation, growth, and coalescence of voids the ductile fracture criterion assumes that the equivalent plastic strain at crack initiation is a function of the stress triaxiality, plastic strain rate $\dot{\varepsilon}_{eq}^{pl}$, and temperature T :

$$4) \quad \varepsilon_{eq_D}^{pl} = F(\eta, \dot{\varepsilon}_{eq}^{pl}, T) .$$

The criterion for damage initiation is met when

$$5) \quad \frac{d\varepsilon_{eq}^{pl}}{F(\eta, \dot{\varepsilon}_{eq}^{pl}, T)} = 1 .$$

There are several models for the crack initiation function $F(\eta, \dot{\varepsilon}_{eq}^{pl}, T)$ [1-5]. Seven fracture models were evaluated and partially calibrated for 2024-T351 aluminum [2]. In the current work, we use the Johnson-Cook [1] criterion primarily, but also consider the Hooputra model [4].

The Johnson-Cook criterion was selected because of the available documented material constants for various materials at large strain, high strain rates, and high temperatures [3]. The documented data is a good starting point for evaluation of material damage initiation in an X100 pipeline steel.

The Johnson-Cook criterion is

$$6) \quad F(\eta, \dot{\varepsilon}_{eq}^{pl}, T) = d_1 + d_2 e^{d_3 \eta} \left(1 + d_4 \ln \frac{\dot{\varepsilon}_{eq}^{pl}}{\varepsilon_0} \right) \left(1 + d_5 \frac{T}{T_{ref}} \right)$$

where ε_0 and T_{ref} are the reference strain rate and reference temperature, respectively, and $d_1 - d_5$ are material constants to be determined

The current experiments were performed at room temperature. Therefore d_5 is 0 and equation 6 reduces to

$$7) \quad F(\eta, \dot{\varepsilon}_{eq}^{pl}, T) = d_1 + d_2 e^{d_3 \eta} \left(1 + d_4 \ln \frac{\dot{\varepsilon}_{eq}^{pl}}{\varepsilon_0} \right) .$$

The Hooputra et al. model is given by

$$8) \quad F(\eta, \varepsilon_{eq}^{pl}, T) = d_0 e^{-c\eta} + d_1 e^{c\eta}.$$

For materials where the fracture strain decreases monotonically with the increase of the stress triaxiality ($d_1 = 0$), Equation 8 reduces to

$$9) \quad F(\eta, \varepsilon_{eq}^{pl}, T) = d_0 e^{-c\eta}.$$

In this model, the crack initiation function does not depend on the strain rate and temperature. However, it is possible to derive different material constants d_0 , d_1 , c for variable temperatures or strain rates:

$$10) \quad F(\eta, \varepsilon_{eq}^{pl}, T) = d_0 \varepsilon_{eq}^{pl, T} e^{-c \varepsilon_{eq}^{pl, T} \eta} + d_1 \varepsilon_{eq}^{pl, T} e^{c \varepsilon_{eq}^{pl, T} \eta}.$$

For orthotropic materials, a more general form has been derived with additional material constants [4].

Following damage initiation, the damage evolution representation consist of two forms: softening of the flow stress and degradation of the elasticity

The solid curve in **Figure 5** represents the damaged stress-strain response, while the dashed curve is the response in the absence of damage.

Fracture/damage advance is characterized by the energy dissipated. The energy can be introduced directly or by the displacement up to complete degradation:

$$11) \quad G_f = \int_{\varepsilon_b^{pl}}^{\varepsilon_f^{pl}} L \sigma d\bar{\varepsilon}^{pl} = \int_0^{u_f^{pl}} \sigma d\bar{u}^{pl}$$

where

G_f is the energy required to open a unit area of a crack, u^{pl} is the equivalent plastic displacement as the crack advances, and L is the characteristic length of an element.

The damage can be characterized either by G_f or by u^{pl} .

Since the computation was performed in an explicit method, stability is required, so computations must converge unconditionally.

For linear elastic materials, based on the element-by-element estimate, the stability limit is defined as

$$12) \quad \Delta t_{stable} \frac{C_d}{L^e} \leq 1, \quad \text{and} \quad C_d = \frac{E}{\rho}$$

where Δt_{stable} is the stable time step, L^e is the smallest element dimension in the mesh, E is the Young modulus, and ρ is the density. This estimate for Δt is based on

linear elastic conditions and is only approximate, and in some cases it is not a conservative estimate.

Derivation of Ductile Damage Parameters

The numerical simulation consists of a combined model for the specimen and the loading grips assembly. Initially, because of symmetry, only a quarter of the assembly was considered. However, gaps exist between the loading pins (**Figure 2**) and the grip plates, and between the loading plates and the grips, and misalignment is possible. To account for such asymmetries a full 3D model was constructed as shown in **Figure 6**.

The assembly was loaded in displacement. The loading force was calculated by integrating the normal stress in the loading direction over the area normal to the loading direction.

The force displacement curves, for the quasi static measurements from the LVDT and CMOD are shown in **Figures 7 and 8** respectively. The displacements measured through the elastic portions of the curves of the LVDT are much higher than the displacements measured with the clip gauge. Examination of the specimens showed the differences were, in part, due to slipping of the specimens in the grips (up to 2 mm slippage in worst case). The remainder of the difference is a result of elasticity in the load line. The combined effect of these experimental factors results in the differences in elastic slopes shown in **Figure 7 and 8**. There is no grip effect and only a slight parasitical elasticity effect associated with the CMOD data. Therefore, for evaluation of the material damage properties, the CMOD experimental results was used. The LVDT data, however, does provide useful information at displacements well beyond the maximum displacement possible for the CMOD gauges used, so these data are included for additional information.

Accurate simulation of damage requires proper material properties. The engineering stress strain curve of undamaged material is available in reference [10] and is plotted in **Figure 9**. The damage behavior is the subject of the current work.

The evaluation of the constants for both the Johnson-Cook [1] and Hooputra [4] models was done by parametric adjustment between the computed and the experimental results. The constants (d_1 , d_2 , d_3 of eq. 7 or d_0 , d_1 , c of eq. 8) were identified by an iterative process. At each iteration cycle a complete simulation of displacement loaded MDCB specimen, up to a fully damaged phase, was carried out. At each time step of the iteration cycle, the stress triaxiality was evaluated by the computed stress field. Subsequently, the material constants and the stress triaxiality were applied to evaluate the equivalent plastic strain. Then the damage initiation, based on the equivalent plastic strain, was used to determine the crack advance.

As a starting point of the parametrical calibration, the damage initiation criteria of the Johnson-Cook model (Equation 7) for HY-100 steel was taken [3]. For each computational cycle, the predicted load displacement curve was compared with the experimental result. At each iteration cycle, the material constants were updated up to an acceptable curve fit, as shown in **Figure 10**. With the fitted computational result, the equivalent plastic strain at damage initiation versus the stress triaxiality was derived for points along the damage propagation path. The results at the initial guess and at the final parametrical fit for both Johnson-Cook [1] and Hooputra et al. [4] models are shown in **Figure 11**.

The fluctuation in the computational result is the outcome of the explicit numerical approach used for the crack initiation and evolution process. The fluctuation can be reduced by reducing the time step Δt_{stable} . However, reducing the time step by half results in significant increases to the overall computational time.

The final fit for the quasi static case resulted in the following values for the Johnson-Cook [1] material constants of equation 7: $d_1=-0.7$, $d_2=2.6$, $d_3=-0.5$, $d_4=0$, and $G_f = 0.02 \text{ J/mm}^2$ (the energy required to open a unit area of a crack). For the Hooputra et al model [4] of equation 8, $d_o=1.95$, $d_o=-0.1$, and $c=0.6$.

High crosshead velocity verification

Since a crack in a pipeline can propagate at high speed, experiments were also carried out with higher crosshead velocities [10]. There were no significant changes from the quasi-static case to crosshead velocities up to 300 mm/s as shown in **Figure 12**. The LVDT data is compared here, because the CMOD clip gages used for the tests could not keep up the rate of the crack mouth opening at the higher velocities. So, although the initial slopes of the LVDT curves should be steeper (as shown in **Figure 10** with CMOD data), the similarity in the curve shape for the quasi-static and dynamic data is clear.

In order to obtain the value of d_4 for the Johnson-Cook criterion in equation 6, a parametric fit of the 300 mm/s experiment was carried out for comparison to the quasi static case. Using a reference strain rate of $\dot{\epsilon}_0 = 1$ and the computed plastic strain rate ($\dot{\epsilon}_{eq}^{pl}$) at the vicinity of the damage, the 300 mm/s data indicates a value for d_4 of 0.017.

The less than 2 % difference between d_4 for the quasi static tests and the 300 mm/sec crosshead velocity tests indicates low accuracy in the evaluation of d_4 . For more accurate estimations, experiments with much higher crosshead velocities will be required. Tests have now been conducted at velocities up to approximately 80 m/s, but reliable load/displacement measurements have not yet been developed. This is a subject for future work.

Validation

In order to validate the computations for crack velocity, the experimental data was compared to the computed values. The computed crack velocity was obtained by analyzing the evolution of the crack extension, differentiating the crack length by the time. Sample pictures of the computed results along the crack propagation are shown in **Figure 13** and plotted in **Figure 14**. The computed crack velocities at a 300 mm/sec crosshead speed are systematically lower than the experimental measurements, but are generally within 85 % of the experimental values.

In addition to the force-displacement and crack velocity, a visual validation between the plotted numerical geometry and captured experimental pictures for quasi static and dynamic tests was performed. The comparisons in **Figures 15 and 16** show good agreement between the appearance of the computed cracks and crack observed in the experiments. The general crack geometry and the fracture morphology are both representative of the “flat” morphology often observed for the quasi static tests.

Summary and Conclusions

- Based on a commercial FEM code, a numerical tool to model dynamic crack propagation was constructed.
- The initiation and evolution of fracture in the CTOA specimens were characterized as ductile with nucleation, growth, and coalescence of voids.
- Failure was characterized by damage initiation at a specific strain based on the Johnson-Cook [1] and Hooputra *et al.* [4] damage models, and material degradation up to specified energy dissipation.
- The failure parameters of the Johnson-Cook and Hooputra *et al.* models were evaluated by parametrical computation. The parameters were altered to adjust the numerically obtained force displacement curve to the experimental results.
- Validation of the model and damage properties was achieved using two approaches.
 - The crack speed, as a function of the crack length was obtained numerically and compared to experimental results. It was found to be 15 % lower than experimental results. Reasons for the low prediction are not clear.
 - Visual validation of the crack shape of the numerical computations showed good agreement with the shape of the crack from the experiments.
- The equivalent plastic strain parameters of damage for both Johnson-Cook and Hooputra *et al.* models were defined for X100 steel and are ready to use for crack simulations in gas pipelines made from that material.

References

1. Johnson G. R. and Cook W. H., Fracture Characteristics of Three Metals Subjected to Various Strains, Strain rates, Temperatures and Pressures, *Engineering Fracture Mechanics*, Vol. 21, no.1, pp. 31–48, 1985.
2. Wierzbicki, T. Bao, Y., Lee, Y., Bai, Y., Calibration and Evaluation of Seven Fracture Models, *Int. J. of Mechanical Sciences*, 47, 2005.
3. Johnson, G. R. and Holmquist T. J., Test Data and Computational Strength and Fracture Constant for 23 Materials Subjected to Large Strain, High Strain Rates, and High Temperatures, Los- Alamos report: LA-11463-MS, 1989.
4. Hooputra H., Gese H., Dell H., and Werner H., A comprehensive failure model for crashworthiness simulation of aluminum extrusions, *Int. J. of Crashworthiness*, Vol. 9, No. 5, 2004.
5. Xue L., Damage accumulation and fracture initiation in uncracked ductile solids subjected to triaxial loading, *Int. J. of Solids and Structures*, 44, 2002.
6. Ph. P. Darcis, C. N. McCowan, E. S. Drexler, J. D. McColskey, A. Shtechman and T. A. Siewert, Fracture Toughness through a Welded Pipeline Section- Crack Tip Opening Angle Criterion, *Welding and Materials – Technical, Economic and Ecological Aspects*, Vol. 51, special July issue, pp.225 -234, 2007
7. Hashemi, S. H., Howard, I. C., Yates, J. R., Andrews, R. M., and Edwards, A. M., “A Single Specimen CTOA Test Method for Evaluating the Crack Tip Opening Angle in Gas Pipeline Steels”, *Proc. 5th International Pipeline Conference*, paper No. IPC04-0610, Calgary, Alberta, Canada, 2004.
8. Shterenlikht, A., Hashemi, S. H., Howard, I. C., Yates, J. R., and Andrews, R. M., “A specimen for studying the resistance to ductile crack propagation in pipes”, *Engineering Fracture Mechanics*, 71, pp. 1997-2013, 2004.
9. Hashemi, S. H., Gay, R., Howard, I. C., Andrews, R. M., and Yates, J. R., Development of a Laboratory Test Technique for Direct Estimation of Crack Tip Opening Angle, *Proc. 15th European Conference of Fracture*, Stockholm, Sweden, 2004.
10. Reuven, R, McCowan, C., Drexler, E., Shtechman, A, Darcis, Ph., Treinen, M., Smith, R., Merritt, J., Siewert, T., and McColskey, J., CTOA Results for X65 and X100 Pipeline Steels: Influence of Displacement Rate, *Proceedings of 7th International Pipeline Conference*, Calgary, Alberta, Canada, 2008.
11. Rudland, D. L., Wilkowski, G.M., Feng, Z., Wang, Y.Y., Horsely, D., and Glover, A. , Experimental investigation of CTOA in pipeline steels, *Engineering Fracture Mechanics*, Vol. 70, pp. 567-577, 2003.
12. O'Donoghue, P. E., Kanninen, M. F., Leung, C. P., Demonofonti, G., and Venzi, S., The development and validation of dynamic fracture propagation

- model for gas transmission pipelines, *Int J. Pres. Ves. and Piping*, Vol. 70, pp. 11-25, 1997.
13. You, X. C., Zhuang, Z., Huo, C. Y., Zhuang, C. J., and Feng, Y. R., Crack arrest in rupturing steel gas pipelines, *International Journal of Fracture*, Vol. 123, pp. 1-14, 2003.
 14. Zienkiewicz, O. C. and Taylor, R. L., *The Finite Element Method*, McGraw-Hill Book Company, 4th Edition, London (1989)
 15. Belytschko, T. and Black, T., "Elastic Crack Growth in Finite Elements with Minimal Remeshing," *International Journal for Numerical Methods in Engineering*, Vol. 45, pp. 601–620, 1999.

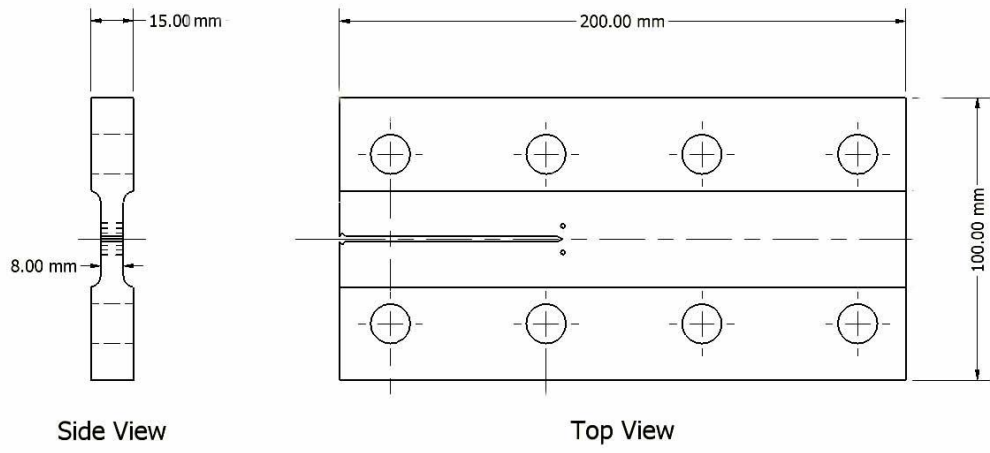


Figure 1: MDCB specimen, configuration and general dimensions.

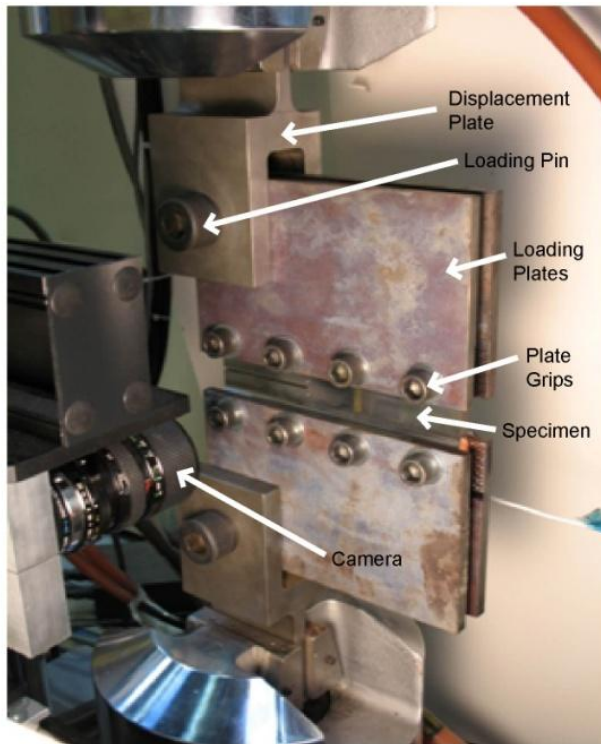


Figure 2: CTOA test set up showing a video camera on a motorized x - y stage (used to follow crack propagation), loading configuration, and stiffening plates on specimen.

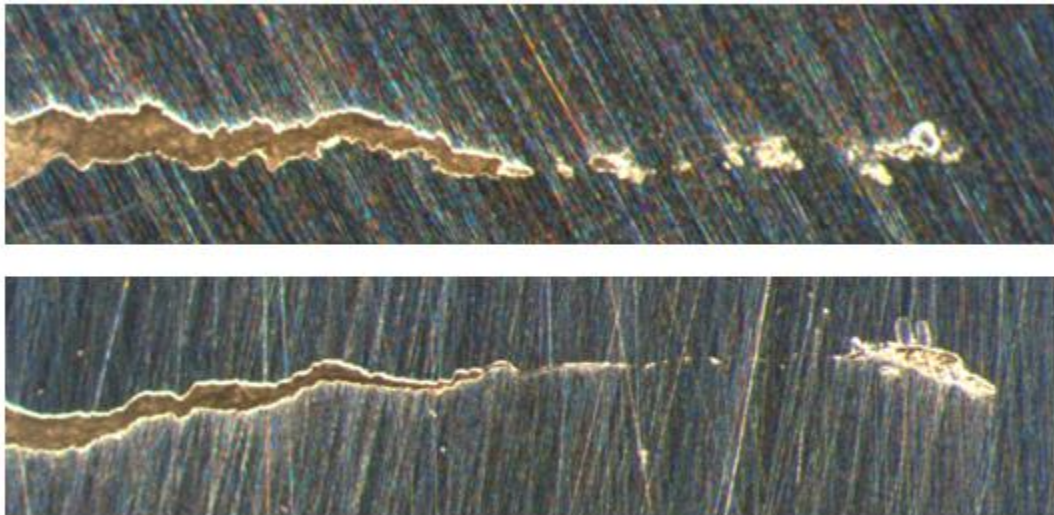


Figure 3: Ductile fracture due to nucleation growth and coalescence of voids in an X100 steel specimen.

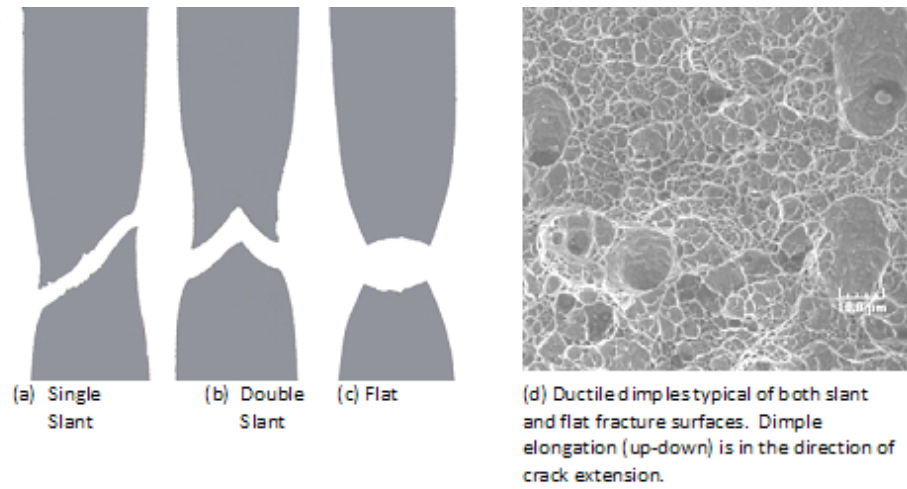


Figure 4: Ductile fracture appearance of the specimens in cross section (a-c), and (d) the ductile dimples characteristic of the fracture surfaces.

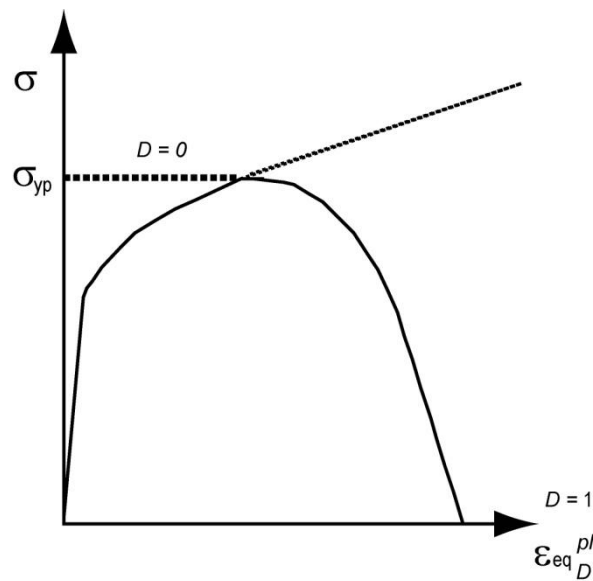


Figure 5: Stress-strain curve with progressive damage degradation (the solid curve in the figure represents the damaged stress-strain response, while the dashed curve is the response in the absence of damage).

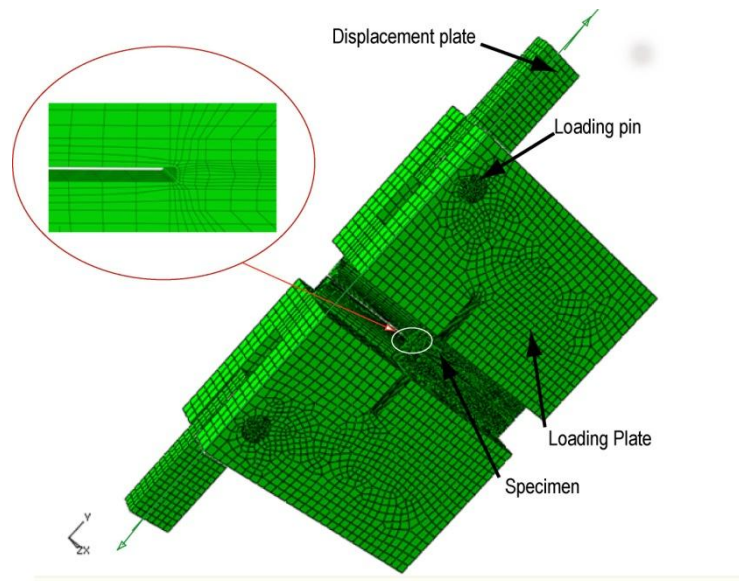


Figure 6. Finite element discretization of the full model.

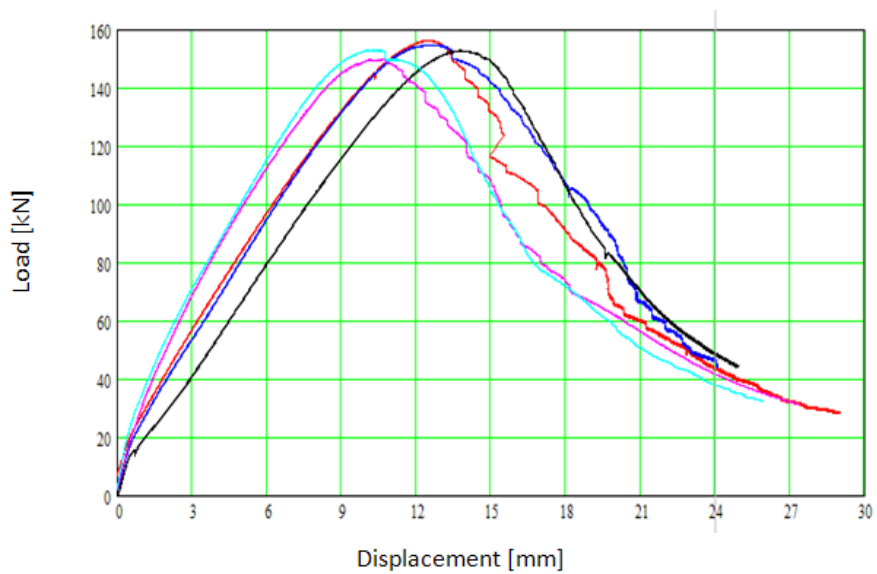


Figure 7: Experimental load displacement curves for LVDT data, showing five results for tests conducted at quasi-static rates ranging from 0.002 mm/s to 0.02 mm/s. Curve shapes are similar for the five results. Variations in elastic slopes of the curves, due to experimental limitations, result in variation of the displacement at maximum load for the tests. However the LVDT curves do provide useful information at high displacements that were not provided by the CMOD gages used.

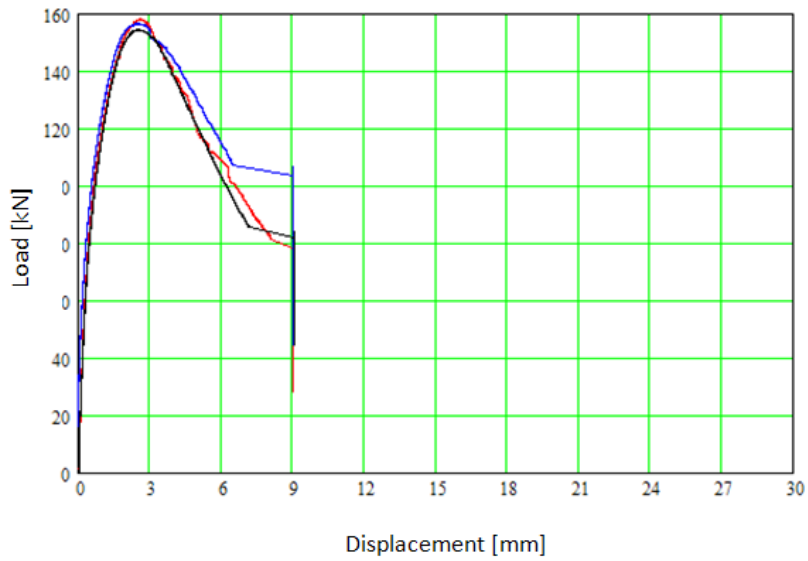


Figure 8: Experimental data for the 3 quasi static tests that had valid CMOD load displacement data. The shapes of the curves and the displacements at maximum load were independent of test rate.

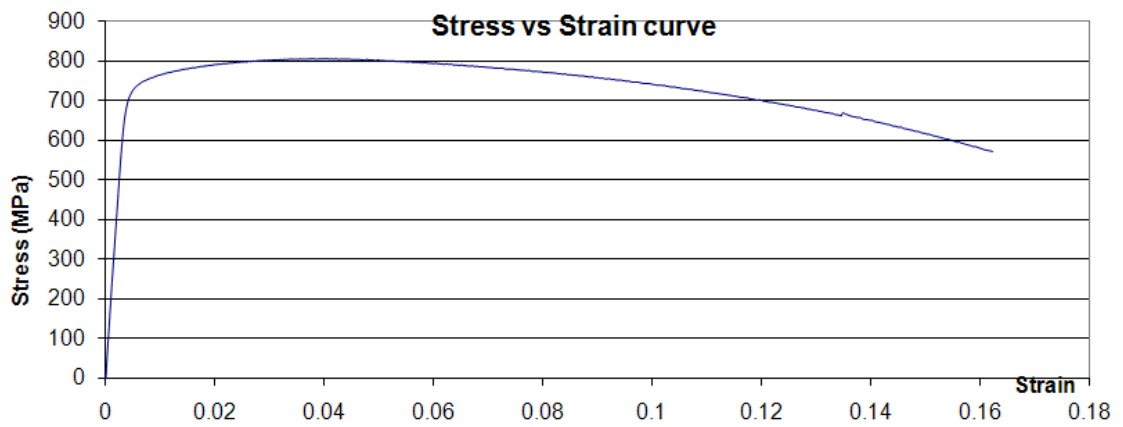


Figure 9: Engineering stress-strain curve for X100 steel [10]

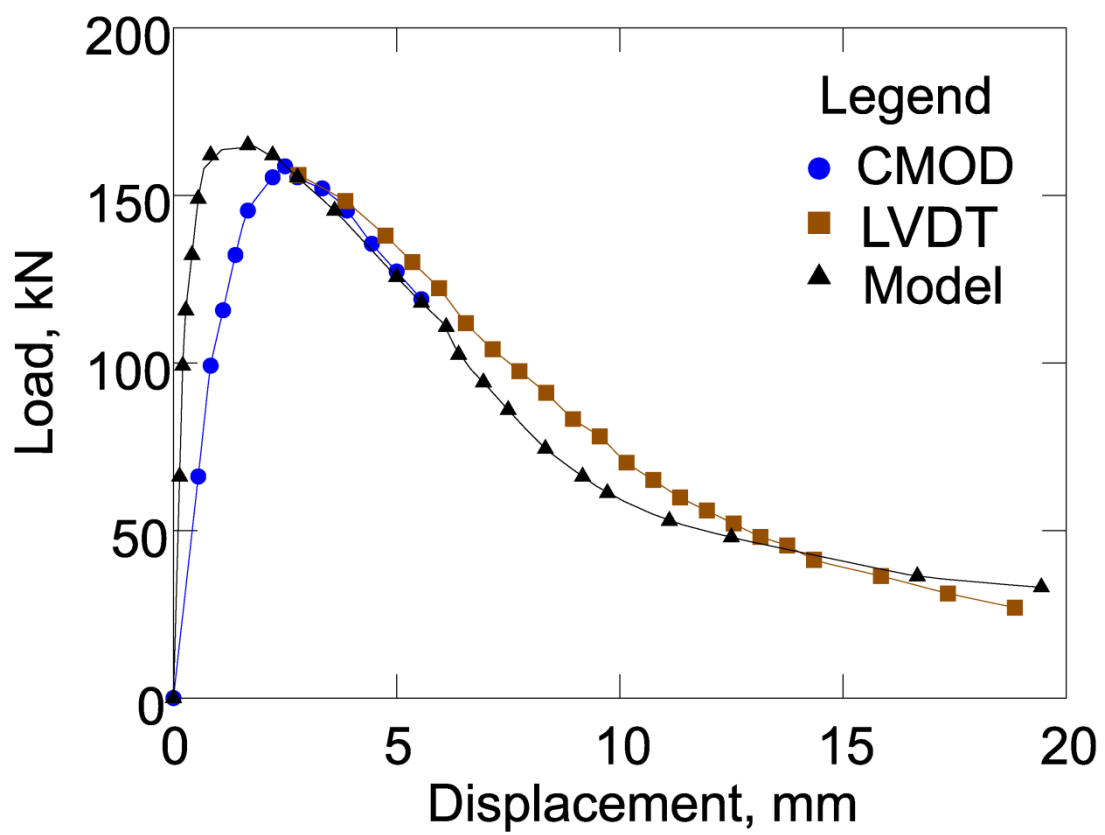


Figure 10: Comparison of the computational result (model) with the experimental CMOD and LVDT load displacement curves. The comparison uses average curves for all three data sets, and the LVDT curve was normalized to align the CMOD and LVDT displacements at peak load.

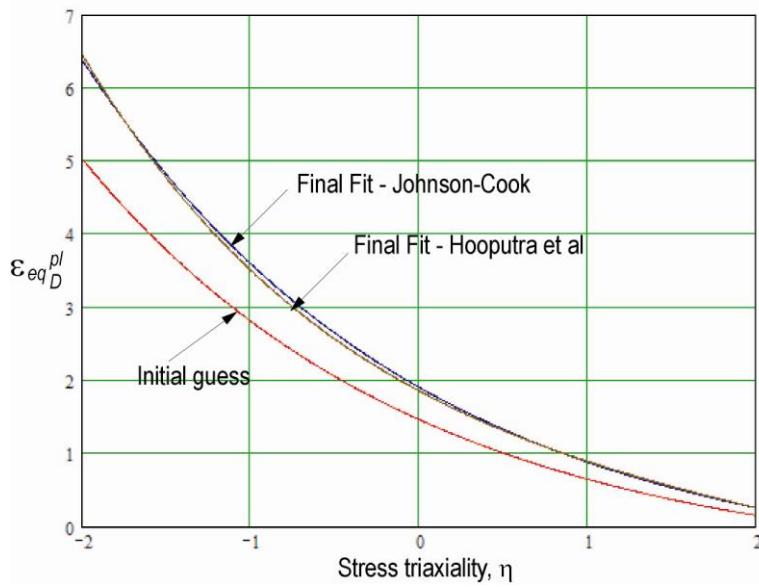


Figure 11: Equivalent plastic strain at damage initiation versus stress triaxiality (as defined in equation 2) for quasi-static (low strain rate) loading.

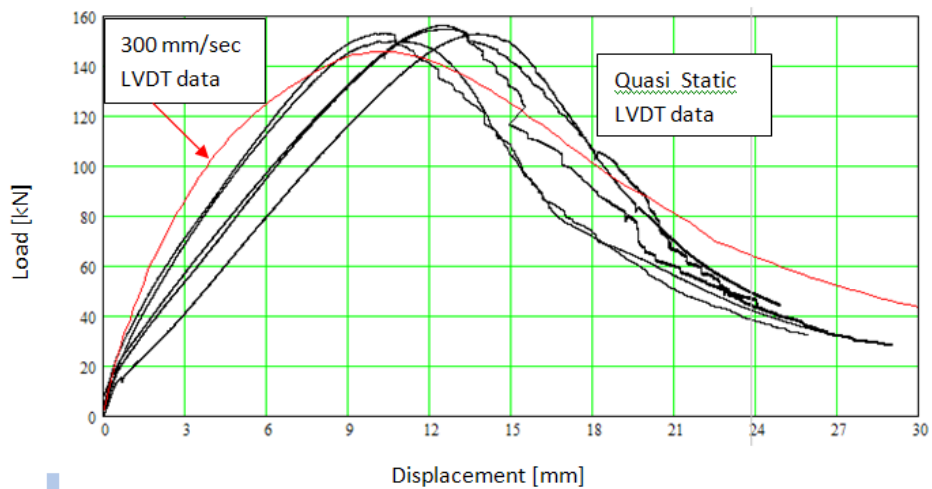


Figure 12: Experimental load displacement curves for a dynamic test (300 mm/s) compared with 5 quasi static tests (0.002 mm/s to 0.02 mm/s). Only LVDT data is compared here, because CMOD data was not available at the 300 mm/s test rate.

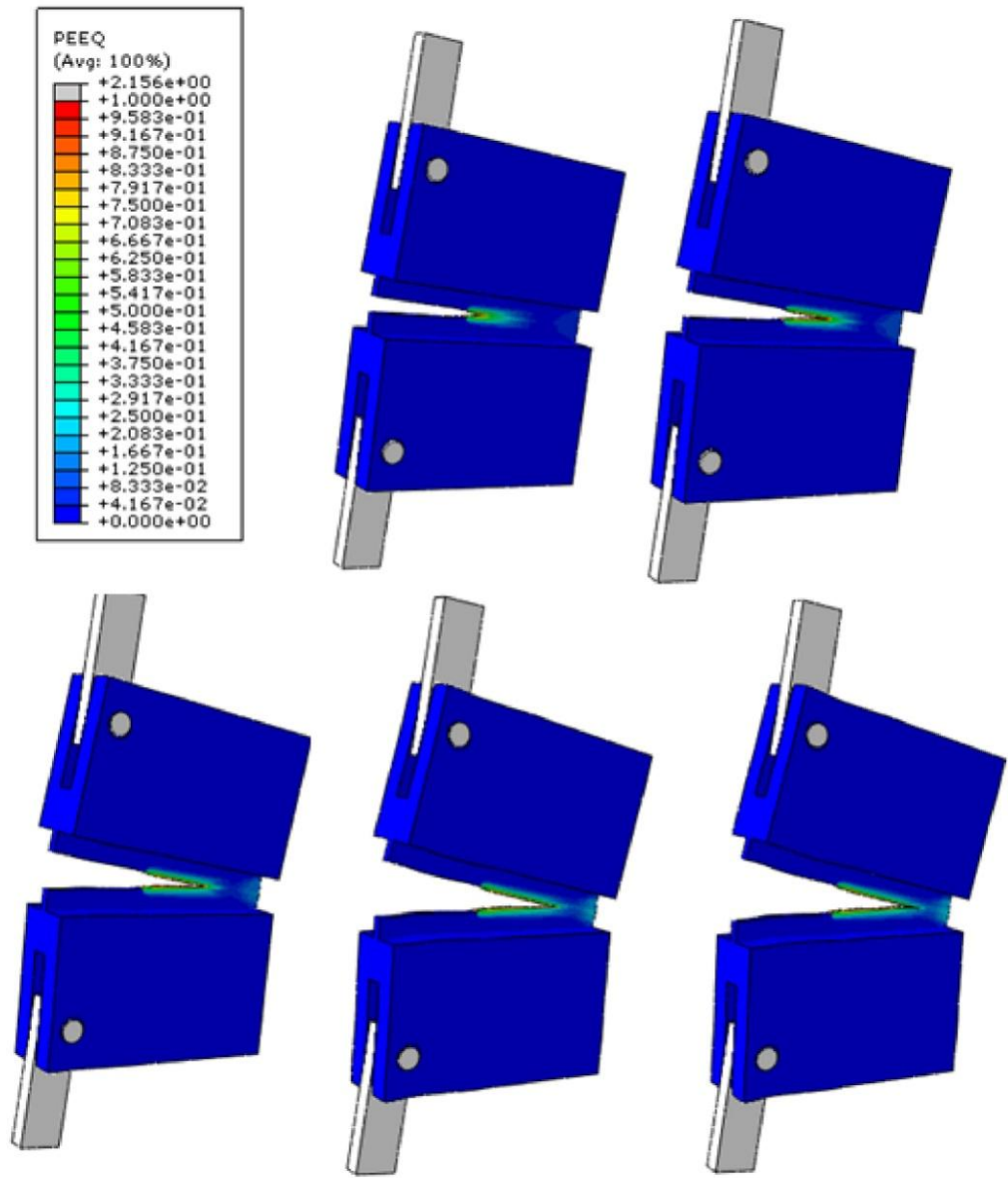


Figure 13: Computed crack evolution, plotted for the equivalent plastic strain (as defined in equation 1).

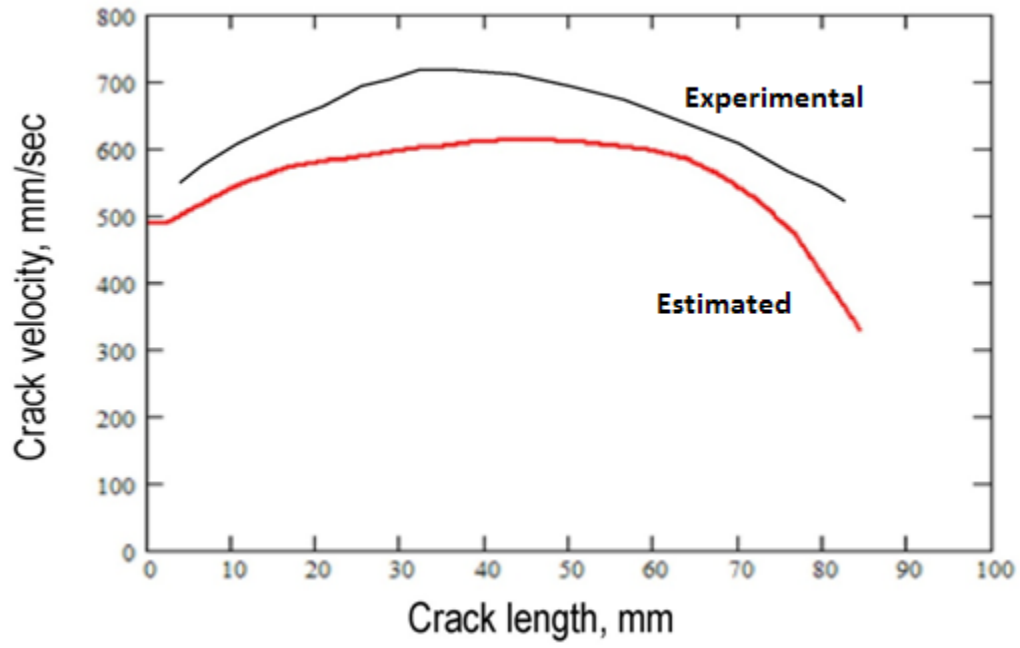


Figure 14: Measured (black) and computed (red) crack velocity versus crack length for the 300 mm/s cross head velocity.

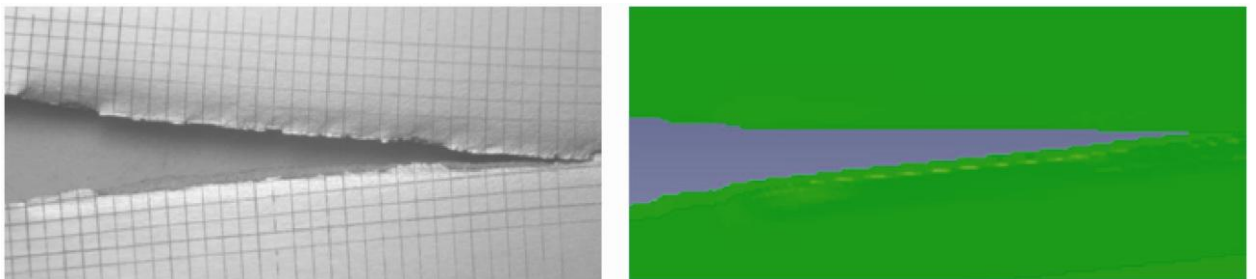


Figure 15: Crack geometry at the circumference of the specimen.

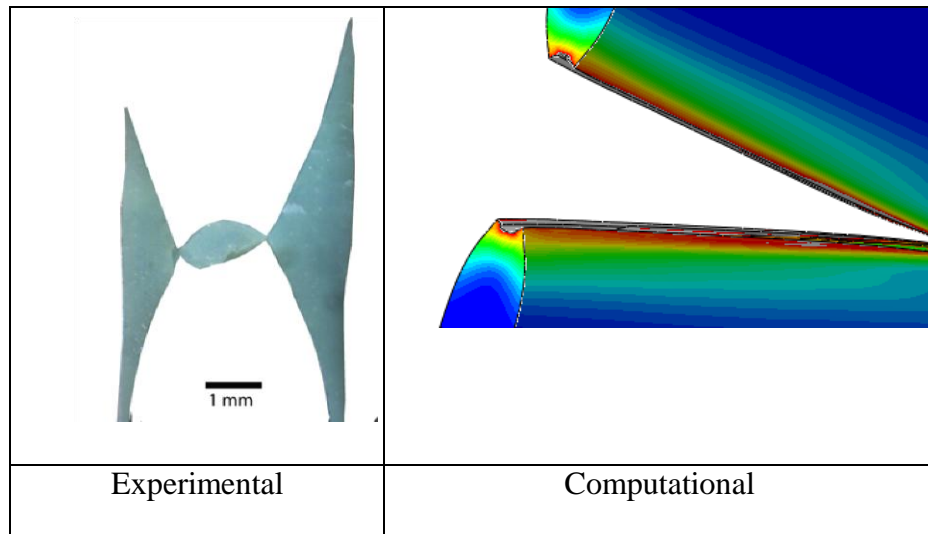


Figure 16: Crack face shape of a casting from a specimen that failed in a “flat” fracture mode compared with the estimated failure appearance computed with the model. The extent of plastic necking at the surface and the curved fracture surface of the computed shape are in good agreement with both this casting and the typical shape for a flat fracture shown in Figure 4.